

Critical Phenomena and the Quantum Critical Point of Ferromagnetic $\text{Zr}_{1-x}\text{Nb}_x\text{Zn}_2$ D. A. Sokolov¹, M. C. Aronson¹, W. Gannon¹, Z. Fisk²¹) University of Michigan, Ann Arbor, MI 48109-1120, USA²) Florida State University,
Tallahassee, FL 32310-3706, USA

We present a study of the magnetic properties of $\text{Zr}_{1-x}\text{Nb}_x\text{Zn}_2$, using an Arrott plot analysis of the magnetization. The Curie temperature T_C is suppressed to zero temperature for Nb concentration $x_c = 0.083 \pm 0.002$, while the spontaneous moment vanishes linearly with T_C as predicted by the Stoner theory. The initial susceptibility displays critical behavior for $x < x_c$, with a critical exponent which smoothly crosses over from the mean field to the quantum critical value. For high temperatures and $x < x_c$, and for low temperatures and $x > x_c$ we find that $\chi = \chi_0 + aT^{-4/3}$, where χ_0 vanishes as $x \rightarrow x_c$. The resulting magnetic phase diagram shows that the quantum critical behavior extends over the widest range of temperatures for $x = x_c$, and demonstrates how a finite transition temperature ferromagnet is transformed into a paramagnet, via a quantum critical point.

PACS numbers: 71.10.Hf, 75.10.Lp, 75.40.Cx

Zero temperature phase transitions and their attendant quantum critical fluctuations have emerged as dominant features in the phase diagrams of different types of strongly correlated electron systems, from oxide superconductors [1] and heavy fermion compounds [2, 3], to low dimensional materials [4]. These fluctuations qualitatively modify the electronic states near a quantum critical point (QCP), leading to unusual temperature divergences of the susceptibility and heat capacity, to anomalous power law behavior in the electrical transport, and even to scale invariance in the magnetic responses [5, 6, 7, 8, 9]. The fundamental excitations near QCPs are qualitatively unlike those of conventional metals, representing in some cases entirely new classes of collective states [10, 11]. A central issue is whether these unusual properties require the exceptionally rich physics of these host systems, derived from low dimensionality and strong correlations, or whether only proximity to a zero temperature phase transition is required. Thus, it is important to identify electronically simple systems, and to study the evolution of their critical phenomena as the ordered phases are suppressed to zero temperature.

Itinerant ferromagnets are particularly attractive hosts for such a study, as they lack the complex interplay of itinerant and localized character found near the QCPs of heavy fermion systems [8, 12]. Pressure and compositional variation have been used to suppress the finite temperature magnetic ordering transition, finding that the magnetically ordered phase can vanish discontinuously as in pressurized MnSi [13], UGe_2 [14], and perhaps ZrZn_2 [15, 16, 17, 18, 19], or continuously as in $(\text{Ni}_{1-x}\text{Pd}_x)_3\text{Al}$ [20]. While disorder can affect the order of the quantum critical phase transition in itinerant ferromagnets [21], it is generally found in systems with continuous transitions tuned by a parameter that the QCP which occurs for $x = x_c$ and $T = 0$ dominates the magnetic phase diagram and generates a phase line $T_C^{(d+n)=z}(x)$

x_c), where $d = 3$, $z = n + 2 = 3$ [13, 19, 22, 23]. Near the QCP, the electronic part of the heat capacity is maximized [24, 25, 26, 27, 28] while the electrical resistivity evolves from $\propto T^{-1}$ for $x = x_c$ to the Fermi liquid $\propto T^2$ for $x > x_c$ [19, 29, 30, 31]. The low field magnetization is anomalous near the QCP [13, 19], but a detailed study spanning the ordered and paramagnetic phases remains lacking. We provide this study of the magnetization of ZrZn_2 here, discussing how the QCP is generated with Nb doping, and the subsequent evolution of the critical phenomena as the QCP is approached.

$\text{Zr}_{1-x}\text{Nb}_x\text{Zn}_2$ is ideal for such a study. Neutron form factor measurements [32] show that the magnetic moment is spatially delocalized, consistent with the small spontaneous moment [33]. We establish a magnetic phase diagram, and show that it is dominated by a QCP at $x_c = 0.083 \pm 0.002$ and $T_C = 0$ K. Stoner theory describes the ferromagnetism of ZrZn_2 well, indicating that variation in the density of states at the Fermi level controls both the Curie temperature T_C and the zero temperature spontaneous moment $m_0(0)$. Our measurements of the initial magnetic susceptibility $\chi(T)$ describe how the critical phenomena evolve with Nb doping, crossing over from mean field behavior when the reduced temperature is low and when Nb concentrations are far from the critical value, to a regime at small $x - x_c$ where the susceptibility is controlled by the QCP over an increasingly broad range of temperatures.

Polycrystalline $\text{Zr}_{1-x}\text{Nb}_x\text{Zn}_2$ samples with Nb concentrations $0 \leq x \leq 0.14$ were prepared by solid state reaction [34]. X-ray diffraction confirmed the C-15 ZrZn_2 structure [33] at each composition, as well as residual amounts of unreacted Zr and Zn. The magnetization was measured using a Quantum Design magnetometer at temperatures from 1.8 K to 200 K and in magnetic fields up to 7 T. The inset of Fig. 1a shows the magnetic isotherms for $\text{Zr}_{1-x}\text{Nb}_x\text{Zn}_2$ ($x = 0.03$) presented as an

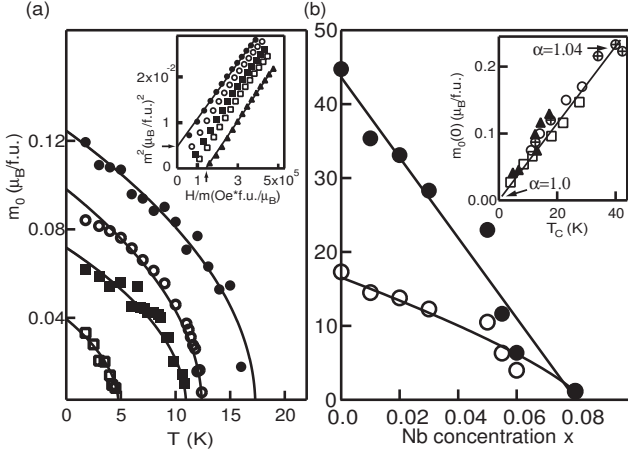


FIG. 1: (a) Temperature dependence of the spontaneous magnetization m_0 in μ_B per formula unit (f.u.) for $Zr_{1-x}Nb_xZn_2$ ($x=0$ (\circ), 0.03 (\square), 0.05 (\triangle), 0.06 (\diamond)). The solid lines are fits to $m_0(T) = m_0(0) [(T_c - T)/T_c]^{0.5}$. Inset: Example of an Arrott plot for $x=0.03$, for temperatures from 1.8 K (\circ) to 20 K (\square), the solid lines are fits to m^2/H , arrows mark extrapolated $1/T$ (horizontal axis) and $m^2(T)$ (vertical axis). (b) Variation of Curie temperature T_c (\circ) and $T_c^{d=3}$ (\square) with Nb concentration x . Solid lines are fits to $T_c/(x_c - x)^{3/4}$ and $T_c^{d=3}/(x_c - x)$, with $x_c = 0.083 \pm 0.002$. Inset: The zero temperature spontaneous moment $m_0(0)/T_c$ vs T_c for Y, Ti, Hf doping (\circ) [37]; pressure, single crystal (\square) [15]; pressure, $ZrZn_{1.9}$ polycrystal (\triangle) [18]; Nb doping, polycrystals, this work (\diamond). Solid line is Stoner parameter [38].

An Arrott plot. Both the spontaneous magnetization $m_0(T) = \lim_{H \rightarrow 0} m(H, T)$ and the initial susceptibility $\chi(T) = \lim_{H \rightarrow 0} dm(H, T)/dH$ were determined by extrapolation of data from fields larger than 4.5 T. Previous de Haas-van Alphen experiments on a single crystal of $ZrZn_2$ found a field induced transition in the magnetization near 5 T [35], and a complex pressure-temperature phase diagram was proposed for this sample [15]. However, our Arrott plots are linear in fields from 1 T – 7 T, at least at low temperatures and for small x , indicating that this field-driven transition is absent, as it was in earlier work [18, 34, 36]. The temperature dependence of $m_0(T)$ is plotted in Fig. 1a, showing that Nb doping continuously reduces T_c and the zero temperature spontaneous moment $m_0(0)$. Fig. 1a shows that for each $x < x_c$, m_0 is described by the mean field expression $m_0(T) = m_0(0) \sqrt{(T_c - T)/T_c}$, where $\beta = 0.5$ and $\gamma = (T_c - T)/T_c$. The suppression of T_c with Nb doping is shown in Fig. 1b, demonstrating that the ferromagnetic phase line obeys the expected $T_c^{(d+n)/z} = T_c^{d=3}/(x - x_c)$ ($d = z = 3$, $n = 1$) [22], terminating at a critical concentration $x_c = 0.083 \pm 0.002$, analogous to the results of high pressure measurements [19].

The suppression of T_c and m_0 with Nb doping indicates that the Stoner theory adequately describes the ferromagnetism in $ZrZn_2$, where the underlying control parameter is the product of the Coulomb interaction

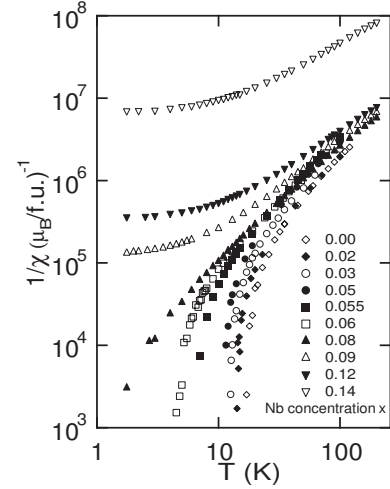


FIG. 2: The temperature dependence of the inverse of the initial susceptibility χ^{-1} for Nb concentrations both larger and smaller than the critical concentration $x_c = 0.083 \pm 0.002$.

and the density of states at the Fermi level. Stoner theory predicts that T_c and $m_0(0)$ are proportional for $\beta = 1$. The inset of Fig. 1b shows this proportionality is valid not only for our Nb doped samples, but also for those with Ti, Hf, and Y doping [37], those with modified stoichiometry [16, 38] and even when high pressures are applied [15, 18, 19]. Values of β are indicated in the inset of Fig. 1b, suggesting that modifications to the underlying electronic structure and not the disorder associated with doping are primarily responsible for altering the stability of ferromagnetism in $ZrZn_2$. Indeed, only a two percent reduction in β is necessary to drive the ferromagnetism in undoped $ZrZn_2$ to the brink of instability, whether by doping or by the application of pressure.

The initial magnetic susceptibility is considerably modified as the system is driven from a finite temperature instability in undoped $ZrZn_2$, through a QCP, and into the paramagnetic phase. Arrott plot analyses are used to deduce $\chi^{-1}(T) = \lim_{H \rightarrow 0} dH/dm(H, T)$ shown in Fig. 2 for a wide range of Nb concentrations x . χ^{-1} diverges at T_c in the ferromagnetic samples ($x < x_c$), with little sign of critical rounding. The sample with $x = 0.08$ displays a nearly power-law response in absolute temperature, as expected near a QCP [22, 39]. Finally, for $x > x_c$, $\chi(T)$ approaches a constant value χ_0 as $T \rightarrow 0$, signalling that long range ferromagnetic order is no longer possible.

The initial susceptibility for $x < x_c$ is well described by a power law $\chi = \chi_0$ over at least two decades of reduced temperature $\gamma = (T - T_c)/T_c$, and for absolute temperatures as large as 100 K (Fig. 3a). The inset of Fig. 3a shows that χ increases smoothly from the near mean field value 1.08 ± 0.05 previously observed in $ZrZn_2$ [36], to 1.33 ± 0.01 for $x > x_c$. Since the interactions which lead to magnetic order in itinerant ferromagnets are long ranged, the intrinsic exponents related to the underlying symme-

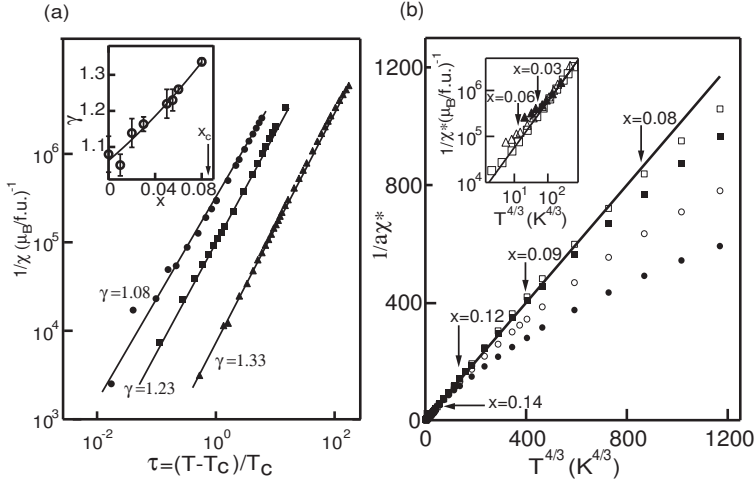


FIG. 3: (a) $1/\chi = \chi_0^{-1}$ at different Nb concentrations: $x=0$ (\circ), $x=0.055$ (\square), $x=0.08$ (\triangle). Solid lines are the best fits to $1/\chi = \chi_0^{-1}$. Inset: the critical exponent (γ) increases continuously as $x \rightarrow x_c$. Solid line is guide for the eye. (b) $1/a\chi^*$ (defined in the text) for $x \geq x_c$ is proportional to $T^{4/3}$ for $T \gg T_c$. For $x \geq x_c$, $1/a\chi^*$ deviates from $T^{4/3}$ (solid line) above a crossover temperature T_m marked by arrows: $x=0.08$ (\circ), $x=0.09$ (\square), $x=0.12$ (\triangle), $x=0.14$ (\diamond). Inset: For $x \geq x_c$, $1/\chi^*$ deviates from $T^{4/3}$ behavior below a crossover temperature T_G marked by arrows: $x=0.08$ (\circ), $x=0.06$ (\square), $x=0.03$ (\triangle). Solid line is best fit of $1/\chi^* = aT^{4/3}$ for $x=0.08$.

tries are only found at reduced temperatures which are much smaller than those accessed in our experiments. [40, 41, 42]. We conclude that the variation of χ with Nb concentration is the result of a gradual crossover from the mean field behavior associated with a finite temperature ferromagnetic transition for $x < x_c$ to quantum criticality as $x \rightarrow x_c$.

Isolating the temperatures and Nb concentrations where χ is dominated by the QCP is straightforward in the paramagnetic regime ($x < x_c$). Near the QCP, the initial susceptibility for an itinerant, three dimensional ferromagnet is given by $\chi = \chi_0^{-1} + aT^{4/3}$, with $\chi_0^{-1} / (x - x_c) \ll 22$. The variation of χ_0^{-1} with Nb concentration x is plotted in the lower panel of Fig. 4. As predicted, χ_0^{-1} vanishes approximately linearly with $(x - x_c)$, while a change by less than 10%. The temperature dependent part of the initial susceptibility is isolated by defining $1/a = (\chi_0^{-1} - \chi_0^{-1}) / T^{4/3}$. $1/a$ is plotted in Fig. 3b as a function of $T^{4/3}$ for each of the three paramagnetic concentrations with $x=0.09, 0.12$, and 0.14 , and for comparison $x=0.08$, which has $T_c = 12.0$ K. Fig. 3b demonstrates that $1/a = T^{4/3}$ below a temperature T_m which vanishes at $x=0.15$ (Fig. 4), the termination of quantum criticality for $x > x_c$.

Quantum criticality is also observed for $x > x_c$, although the critical phenomena associated with the finite temperature ferromagnetic transition ultimately dominate as $T \rightarrow T_c$. Since $\chi = \chi_0^{-1} + aT^{4/3}$, with $\chi_0^{-1} / (x -$

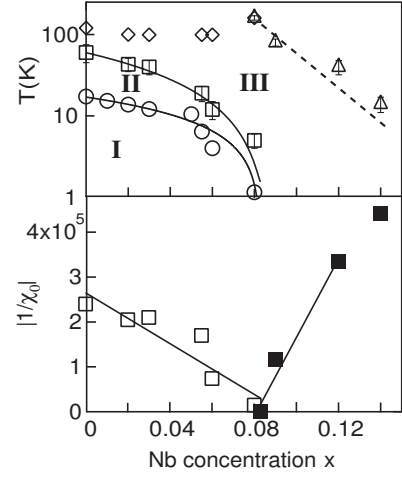


FIG. 4: Top: The temperature - Nb concentration phase diagram for $Zn_{1-x}Nb_xZn_2$. $T_c(x)$ (\circ), with the phase line $T_c / (x - x_c)^{3/4}$, the crossover temperature T_G (\diamond) for $x \geq x_c$ with the crossover line $T_G / (x - x_c)^{1.2 \pm 0.3}$, the crossover temperature T_G (\triangle) for $x \geq x_c$, dashed line is a guide for the eye. (\square) indicate the highest temperature investigated for $x \geq x_c$. I, II, and III correspond, respectively, to the region of stable ferromagnetism, the crossover region, and the quantum critical region as defined in the text. Bottom: Variation with Nb concentration of the $T=0$ inverse susceptibility $1/\chi_0$ for $x < x_c$ (\circ) and for $x \geq x_c$ (\square). Solid lines are fits with $1/\chi_0 = a(x - x_c)$. For $x=0.14$, $1/\chi_0$ is divided by 15 to appear on the plot.

x_c), the quantum critical susceptibility is largest for $x \geq x_c$, and extends over the broadest range of absolute temperatures, since $T_c \rightarrow 0$. This is demonstrated in the inset of Fig. 3b, where we have plotted $1/\chi = \chi_0^{-1} + aT^{4/3}$ as a function of $T^{4/3}$. For $x \geq x_c$, the $T^{4/3}$ behavior is only found above a temperature T_G which grows rapidly with $(x - x_c)$, as shown in Fig. 4. The lower panel of Fig. 4 shows that for $x \geq x_c$, $1/\chi_0$ decreases approximately linearly with $(x - x_c)$, while the magnitude a of the $T^{4/3}$ term is approximately independent of x , as in the paramagnetic phase $x > x_c$.

Our magnetization measurements establish that the phase diagram of $Zn_{1-x}Nb_xZn_2$ has three different regions, depicted in Fig. 4. Ferromagnetic order is found in Region I, below a phase line $T_c(x)$ which is controlled by the $x = x_c$, $T_c = 0$ QCP. The Stoner criterion which describes the stability of ferromagnetism remains unchanged even as $x \rightarrow x_c$, indicating that the reduction in the electronic density of states drives the QCP. The spontaneous moment obeys the mean field expression, $m_0(x) = m_0(0)^{0.5}$ in Region I.

Simple power law divergences with reduced temperature are found in Region II, ($\chi = \chi_0$), and the enhancement of χ as $x \rightarrow x_c$ reveals that Region II is best considered a crossover region, controlled by the relative magnitudes of χ_0 and $(x - x_c)$. Specifically, for small and large $(x - x_c)$, we find the mean field behavior of

a finite transition temperature ferromagnet¹. In the opposite limit (small $(x-x_c)$ and large T) we find that the QCP is dominant, yielding $\chi^{-1} \propto a + bT^{4/3}$. Accordingly, it is possible to identify the quantum critical behavior of a three dimensional ferromagnet $\chi^{-1} = \chi_0^{-1} + aT^{4/3}$ above a temperature T_G which decreases rapidly as $x \rightarrow x_c$.

The quantum critical regime III is also extensive for paramagnetic concentrations $x > x_c$, occurring below a temperature T which is almost 150 K for $x = x_c$, and dropping rapidly at larger x . Region III extends to the highest temperatures investigated for $x < x_c$. We speculate that the boundary of the quantum critical regime for $x = x_c$ coincides with the condition that the correlation length is reduced to some minimal length, such as the lattice constant. The phase diagram suggests that this occurs at $T = 0$ for $x \approx 0.15$, but at increasingly high temperatures T as x approaches x_c from above.

The quantum critical behavior documented in this work is in excellent agreement with theoretical predictions for a three dimensional $T_c = 0$ ferromagnet. The $T_c = 0, x = x_c$ QCP affects a surprisingly broad area of the x - T phase diagram, competing with the conventional critical phenomena for even $x < x_c$. We find no indication of new collective phases near the QCP in $Zn_{1-x}Nb_xZn_2$, and suggest that further measurements at lower temperatures and with refined samples would be very interesting to further pursue this issue.

Work at the University of Michigan was performed under grant NSF-DMR-0405961. Work at FSU was supported by NSF-DMR-0433560. We acknowledge useful conversations with A. J. M. Illis, M. B. Maple, K. V. Kamenev, M. E. J. Newman and L. Sander, as well as the hospitality and support of J. E. Crow and the National High Magnetic Field Laboratory in Tallahassee during the early stages of this work.

[1] J. Orenstein and A. J. M. Illis, *Science* 288, 468 (2000).
 [2] S. Doniach, *Physica* 91B, 231 (1977).
 [3] G. R. Stewart, *Rev. Mod. Phys.* 73, 797 (2001).
 [4] V. J. Emery in *Highly Conducting One-Dimensional Solids*, ed. J. T. Devreese, R. P. Evrard, and V. E. van Doren (New York, Plenum, 1979) p. 247.
 [5] W. M. Ontfroot, M. C. Aronson et al., *Phys. Rev. Lett.* 91, 087202 (2003).
 [6] M. C. Aronson et al., *Phys. Rev. Lett.* 87, 197205 (2001).

[7] M. C. Aronson et al., *Phys. Rev. Lett.* 75, 725 (1995).
 [8] A. Schroder et al., *Nature* (London) 407, 351 (2000).
 [9] S. M. Hayden et al., *Phys. Rev. Lett.* 66, 821 (1991).
 [10] R. B. Laughlin et al., *Proc. Nat. Acad. Sci.* 97, 32 (2000).
 [11] T. Senthil et al., *Science* 303, 1490 (2004).
 [12] Q. Si et al., *Nature* 413, 804 (2001).
 [13] C. P. Eiderer et al., *Phys. Rev. B* 55, 8330 (1997).
 [14] C. P. Eiderer and A. D. Huxley, *Phys. Rev. Lett.* 89, 147005 (2002).
 [15] M. Uhlir et al., *Phys. Rev. Lett.* 93, 256404 (2004). It has subsequently been shown that samples of this type are nonstoichiometric, especially near their surfaces (E. A. Yelland et al., cond-mat/0502341). The elevated Curie temperature of these samples may also be a signature of Zn deficiency [16]. The pressure driven QCP in near-stoichiometric $ZrZn_2$ was previously shown to be second order [17, 18, 19].
 [16] G. S. Knapp et al., *J. Appl. Phys.* 42, 1341 (1971).
 [17] T. F. Smith et al., *Phys. Rev. Lett.* 27, 1732 (1971).
 [18] J. G. Huber et al., *Solid State Commun.* 16, 211 (1975).
 [19] F. M. Grosche et al., *Physica B* 206-207, 20 (1995).
 [20] M. Sato, *J. Phys. Soc. Japan* 39, 98 (1975).
 [21] D. Belitz, T. R. Kirkpatrick, *Phys. Rev. Lett.* 89, 247202 (2002).
 [22] A. J. M. Illis, *Phys. Rev. B* 48, 7183 (1993).
 [23] S. R. Julian et al., *J. Phys.: Condensed Matter* 8, 9675 (1996).
 [24] J. D. Thompson et al., *Physica B* 161, 317 (1989).
 [25] H. Wada et al., *J. Phys. Soc. Japan* 59, 2956 (1990).
 [26] C. J. Fuller et al., *J. Appl. Phys.* 73, 5338 (1993).
 [27] N. Tatewaka et al., *J. Phys.: Condensed Matter* 13, L17 (2001).
 [28] R. Vollmer et al., *Physica B* 312-313, 112 (2002).
 [29] G. Omer et al., *J. Alloys and Compounds* 271-273, 482 (1998).
 [30] C. P. Eiderer et al., *Nature* 414, 427 (2001).
 [31] M. J. Steiner et al., *Physica B* 329-333, 1079 (2003).
 [32] S. J. Pickart et al., *Phys. Rev. Lett.* 12, 444 (1964).
 [33] B. T. Matthias and R. M. Bozorth, *Phys. Rev.* 109, 604 (1958).
 [34] S. Ogawa and N. Sakamoto, *J. Phys. Soc. Japan* 22, 1214 (1967).
 [35] N. Kimura et al., *Phys. Rev. Lett.* 92, 197002 (2004).
 [36] M. Seeger et al., *J. Magn. Magn. Mater.* 139, 312 (1995).
 [37] Shinji Ogawa, *J. Phys. Soc. Japan* 25, 109 (1968).
 [38] G. S. Knapp, *J. Appl. Phys.* 41, 1073 (1970).
 [39] G. G. Lonzarich, in *Electron* edited by M. Springford (Cambridge University Press, Cambridge, England, 1997).
 [40] M. Seeger and H. Kronmüller, *J. Magn. and Magn. Mater.* 78, 393 (1989).
 [41] S. N. Kaul, *J. Magn. and Magn. Mater.* 53, 5 (1985).
 [42] M. Seeger et al., *Phys. Rev. B* 51, 12585 (1995).